J. Fluid Mech. (2008), *vol.* 603, *pp.* 137–149.
doi:10.1017/S0022112008000852 Printed in the United Kingdom

Poiseuille flow in a fluid overlying a porous medium

ANTONY A. HILL AND BRIAN STRAUGHAN
Department of Mathematics, University of Durham, Durham, DH1 3LE, UK

(Received 26 June 2007 and in revised form 31 January 2008)

This paper numerically investigates the instability of Poiseuille flow in a fluid overlying a porous medium saturated with the same fluid. A three-layer configuration is adopted. Namely, a Newtonian fluid overlying a Brinkman porous transition layer, which in turn overlies a layer of Darcy-type porous material. It is shown that there are two modes of instability corresponding to the fluid and porous layers, respectively. The key parameters which affect the stability characteristics of the system are the depth ratio between the porous and fluid layers and the transition layer depth.

1. Introduction

The instability of parallel flows and in particular Poiseuille or Couette flow has been a major problem in fluid mechanics for a long time. Extensive coverage of the early work on such problems is given by Drazin & Reid (1981, chap. 4). More recent work has concentrated on eigenvalue studies in an attempt to reconcile discrepancies between theoretical and experimental results (see e.g. Gustavsson 1986; Butler & Farrell 1992; Friedlander & Howard 1998; Straughan 1998, chap. 8). In this paper, we address the problem of Poiseuille flow when a Newtonian fluid overlies a porous material saturated with the same fluid. The instability for this problem was first addressed by Chang, Chen & Straughan (2006).

The problem of fluid flow over a porous medium has a rich history, especially in connection with thermal convection (see e.g. Nield 1977, 1983, 1991, 1998; Chen & Chen 1988; Straughan 2002; Carr & Straughan 2003; Carr 2004; Chang 2005, 2006; Nield & Bejan 2006; Hirata *et al.* 2007). A key finding was made by Chen & Chen (1988) who employed a Navier–Stokes fluid overlying a Darcy porous medium and discovered that the linear instability curves for the onset of thermal convection may be bi-modal. Their work hinges on the parameter $\hat{d}$ which is defined by

$$\hat{d} = \frac{d}{d_m} = \frac{\text{depth of fluid layer}}{\text{depth of porous layer}}. \tag{1.1}$$

Chen & Chen (1988) discovered that when $\hat{d} \leqslant 0.13$, the instability commences in the porous layer and is dominated by that medium, whereas when $\hat{d}$ is greater than this value, instability is dominated by the fluid layer. This switching of instability by the fluid or porous layer is manifested mathematically by the neutral curve having two local maxima (or minima) which change with variation of $\hat{d}$ to yield a global maximum. This was a major departure from the classical Bénard problem where only one turning point is found.

The reason for studying flow of a fluid overlying a porous medium is the numerous applications in industry and to geophysical problems. Many of these are discussed in

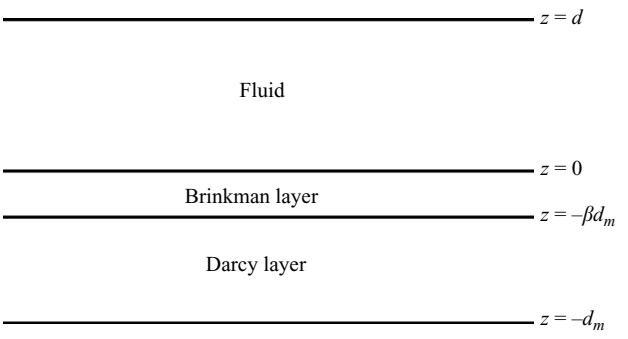

FIGURE 1. Three-layer configuration for Poiseuille flow.

Nield (1977, 1983, 1991, 1998), Nield & Bejan (2006), and in the numerical papers of Choi & Waller (1997), Das, Nassehi & Wakeman (2002), Discacciati, Miglio & Quarteroni (2002) and Miglio, Quarteroni & Saleri (2003). Of particular relevance here are Nield (1983, 1991, 1998) and Lu & Chen (1997) where the question of which porous model is most appropriate (Darcy, Forchheimer, Brinkman) is posed.

The instability problem studied by Chang *et al.* (2006) considered Poiseuille flow of a Newtonian fluid overlying a Darcy porous medium saturated with the same fluid. In addition to two modes of instability corresponding to the porous and fluid layers, respectively, Chang *et al.* (2006) found a third mode which they attributed to a shear layer at the interface. This mode was important and for certain parameter values could dominate the instability. Motivated by (Nield 1983, p. 45), who suggested the use of a Brinkman equation in the boundary-layer region where the fluid enters the porous medium, we here reconsider the Poiseuille-flow instability problem when we have a three-layer configuration (see figure 1). We have a Newtonian fluid overlying a transition layer composed of a Brinkman porous material which in turn overlies a layer of porous material of Darcy type. We believe such a study is timely, especially since Goharzadeh, Khalili & Jorgensen (2005) address precisely this problem from an experimental viewpoint. They raise the important question as to what is the extent of the Brinkman layer, i.e. how deep is the transition layer? If the transition layer depth is δ_1, κ is permeability and D is a typical grain diameter, they conclude that the transition-layer thickness is of the order of the grain diameter, i.e. $\delta_1/D = O(1)$, which was theoretically predicted by Goyeau *et al.* (2003). (In this paper the transition depth is denoted by $\beta d_m \equiv \delta_1$.) This is striking and they also conclude $\delta_1/\sqrt{\kappa} = O(50)$ (which was theoretically predicted by Ochoa-Tapia & Whitaker 1995) whereas previously it had been thought that δ_1 was of the same order as $\sqrt{\kappa}$. We use the important findings of Ochoa-Tapia & Whitaker (1995), Goyeau *et al.* (2003) and Goharzadeh *et al.* (2005) to suggest parameter values for our transition layer. Our findings are notably different from those of Chang *et al.* (2006). In particular, we see that the effect of the third mode effectively disappears when the transition layer is introduced. Also, we find that a key parameter is the depth of the transition (Brinkman) layer. This aspect is discussed in detail in § 3.4.

2. The governing equations

We consider a fluid occupying the three-dimensional layer $\{(x, y) \in \mathbb{R}^2\} \times \{z \in (0, d)\}$, with a homogeneous porous medium occupying the layer $\{(x, y) \in \mathbb{R}^2\} \times \{z \in (-d_m, 0)\}$. The interface between the porous medium and the fluid is at $z = 0$. The

governing equations in the fluid are given by the Navier–Stokes equations

$$\frac{\partial u_i}{\partial t} + u_j \frac{\partial u_i}{\partial x_j} = -\frac{1}{\rho}\frac{\partial p}{\partial x_i} + \nu \Delta u_i, \tag{2.1}$$

$$\frac{\partial u_i}{\partial x_i} = 0. \tag{2.2}$$

Equations (2.1) and (2.2) are assumed to hold for time $t > 0$. In these equations, u_i and p are velocity and pressure, and ρ and ν are density and kinematic viscosity. Standard index notation is employed throughout, with the symbol Δ representing the Laplace operator.

The porous medium is divided into two layers; namely $z \in (-d_m, -\beta d_m)$, which will be referred to as the Darcy layer, and $z \in (-\beta d_m, 0)$, which will be referred to as the Brinkman layer, where $\beta \in (0, 1)$. Note that we define the porosity ϵ to be constant throughout the porous medium. The governing equations in the Brinkman layer are those of the Brinkman model

$$\frac{\rho}{\epsilon}\frac{\partial u_i^b}{\partial t} = -\frac{\partial p^b}{\partial x_i} + \mu_e \Delta u_i^b - \frac{\mu}{\kappa} u_i^b, \tag{2.3}$$

$$\frac{\partial u_i^b}{\partial x_i} = 0, \tag{2.4}$$

for time $t > 0$, in the spatial region $\{(x, y) \in \mathbb{R}^2\} \times \{z \in (-\beta d_m, 0)\}$. In these equations, the variables u_i^b and p^b are the superficial average velocity (or Darcy velocity or filtration velocity) and fluid phase intrinsic average pressure, where μ_e, μ, κ and ρ are effective viscosity, dynamic viscosity, permeability and density, respectively. The parameter β may be varied to assess the effect of the depth of the transition layer. In order to evaluate μ_e, we adopt the approach of Whitaker (1986), where $\mu/\mu_e = \epsilon$. Although this relation is employed throughout the paper, owing to the well-documented challenges in evaluating the actual effective viscosity, variations in μ/μ_e are explored numerically in § 3.5.

The Darcy layer occupies the spatial region $\{(x, y) \in \mathbb{R}^2\} \times \{z \in (-d_m, -\beta d_m)\}$, where the governing equations are those of Darcy flow,

$$\frac{\rho}{\epsilon}\frac{\partial u_i^m}{\partial t} = -\frac{\partial p^m}{\partial x_i} - \frac{\mu}{\kappa} u_i^m, \tag{2.5}$$

$$\frac{\partial u_i^m}{\partial x_i} = 0, \tag{2.6}$$

for time $t > 0$, where the variables u_i^m and p^m are the superficial average velocity and fluid-phase intrinsic average pressure.

The derivation of appropriate boundary conditions at the interfaces is non-trivial. We assume the continuity of normal stresses at the two interfaces. This yields the two interface conditions,

$$-p + 2\mu \frac{\partial u_3}{\partial z} = -p^b + 2\mu_e \frac{\partial u_3^b}{\partial z} \qquad \text{at} \quad z = 0, \tag{2.7}$$

$$-p^m = -p^b + 2\mu_e \frac{\partial u_3^b}{\partial z} \qquad \text{at} \quad z = -\beta d_m. \tag{2.8}$$

This does not mean that the pressure is discontinuous at the respective interfaces. In the porous medium, we interpret the pressure as a pore-averaged pressure and so conditions (2.7), (2.8) are consistent with continuous pressure in the fluid on the

microscopic level. However, we observe that both Chang *et al.* (2006) and ourselves have employed conditions of continuity of pressure in (2.7), (2.8) and we found little variation in our numerical results. Therefore, we believe the interface conditions (2.7), (2.8) are acceptable. In addition to (2.7), we assume the velocity is continuous at $z=0$, i.e. $u_i = u_i^b$. Similarly at $z=-\beta$, we have the continuity of normal velocities such that $u_3^m = u_3^b$. Allowing the continuity of tangential stresses on the interface $z=0$, yields the condition

$$\mu\left(\frac{\partial u_\gamma}{\partial z}+\frac{\partial u_3}{\partial x_\gamma}\right)=\mu_e\left(\frac{\partial u_\gamma^b}{\partial z}+\frac{\partial u_3^b}{\partial x_\gamma}\right)\qquad \text{at}\quad z=0, \tag{2.9}$$

for $\gamma=1,2$. The remaining interface boundary condition must be defined at the interface between the Darcy and Brinkman layers at $z=-\beta$. The stress vector on this interface as approached from the Brinkman layer is

$$t_i^b = n_j t_{ji} = -p^b n_i + 2\mu_e d_{ij}^b n_j,$$

where $\boldsymbol{n}=(0,0,1)$ is the unit normal from the Brinkman layer. Thus, the tangential component of the stress vector, t_γ, $\gamma=1,2$ is given by

$$t_{3\gamma}^b = 2\mu_e d_{\gamma 3}^b = \mu_e\left(u_{\gamma,3}^b + u_{3,\gamma}^b\right).$$

This leads to the Jones (1973) boundary conditions

$$\frac{\partial u_\gamma^b}{\partial z}+\frac{\partial u_3^b}{\partial x_\gamma}=\frac{\alpha}{\sqrt{\kappa}}\left(u_\gamma^b-u_\gamma^m\right)\qquad(\gamma=1,2), \tag{2.10}$$

where α is a constant which depends on the porous medium. We could omit the term $\partial u_3^b/\partial x^\gamma$ on the left-hand side of (2.10) and this would amount to using a Beavers & Joseph (1967) boundary condition. Straughan (2002) found that the Jones and Beavers–Joseph boundary conditions led to almost the same numerical results. We believe this is true here and so employ the invariant condition (2.10).

2.1. *The basic flow*

To introduce Poiseuille flow into the model, we assume a constant pressure gradient in the x-direction. The basic solution, denoted by $(\overline{u}_i,\ \overline{p})$, $(\overline{u}_i^b,\ \overline{p}^b)$ and $(\overline{u}_i^m,\ \overline{p}^m)$, is derived using the aforementioned boundary conditions, together with $\boldsymbol{u}=0$ at $z=d$ and $u_3^m=0$ on $z=-d_m$. This yields,

$$\begin{aligned}\overline{u}(z) &= \tfrac{1}{2}c_1 z^2 + c_2 z + c_3,\\ \overline{u}^b(z) &= c_4 \mathrm{e}^{fz/\sqrt{\kappa}} + c_5 \mathrm{e}^{-fz/\sqrt{\kappa}} - \kappa c_1,\\ \overline{u}^m &= -\kappa c_1,\end{aligned}$$

where $f=\sqrt{\mu/\mu_e}$ $(=\sqrt{\epsilon}$, using Whitaker 1986),

$$\begin{aligned}c_1 &= \frac{1}{\mu}\frac{\mathrm{d}p}{\mathrm{d}x}, \qquad c_2 = Ac_1(\kappa-\tfrac{1}{2}d^2)((f+\alpha)\mathrm{e}^{2\beta f d_m/\sqrt{\kappa}}-(f-\alpha)),\\ c_3 &= \frac{-A}{2}\sqrt{\kappa}c_1 d((f+\alpha)\mathrm{e}^{2\beta f d_m/\sqrt{\kappa}}(fd+2\sqrt{\kappa})+(f-\alpha)(fd-2\sqrt{\kappa})),\\ c_4 &= Afc_1\sqrt{\kappa}(\kappa-\tfrac{1}{2}d^2)(f+\alpha)\mathrm{e}^{2\beta f d_m/\sqrt{\kappa}}, \qquad c_5 = Afc_1\sqrt{\kappa}(\kappa-\tfrac{1}{2}d^2)(f-\alpha),\end{aligned}$$

and $1/A=(f+\alpha)(f\sqrt{\kappa}+d)\exp[2\beta f d_m/\sqrt{\kappa}]+(f\sqrt{\kappa}-d)(f-\alpha)$. To facilitate the interpretation of the relative magnitudes of velocity, the length scales in the fluid and porous layers are normalized by dividing by d and d_m, respectively, and the

dimensional basic velocities in both layers are normalized by dividing by V, the maximum of $\overline{u}(z)$. This yields the velocity function

$$U(z) = \frac{\overline{u}}{V} = \frac{4M_1(\hat{d}M_3\sqrt{\delta} - M_1\hat{d}^2z^2 - \hat{d}M_2z)}{M_2^2 + 4\hat{d}M_3M_1\sqrt{\delta}}, \tag{2.11}$$

for the fluid layer, $z \in (0, 1)$,

$$U_b(z) = \frac{\overline{u}^b}{V} = \frac{4M_1\big(2\delta M_1 - f\sqrt{\delta}(2\delta - \hat{d}^2)\big((f+\alpha)\mathrm{e}^{(f/\sqrt{\delta})(z+2\beta)} + (f-\alpha)\mathrm{e}^{-fz/\sqrt{\delta}}\big)\big)}{M_2^2 + 4\hat{d}M_3M_1\sqrt{\delta}}$$

for the Brinkman layer, $z \in (-\beta d_m, 0)$, and

$$U_m = \frac{\overline{u}^m}{V} = \frac{8\delta M_1^2}{M_2^2 + 4\hat{d}M_3M_1\sqrt{\delta}}$$

for the Darcy layer, $z \in (-d_m, -\beta d_m)$, where $\delta = \kappa/d_m^2$ is the Darcy number, and

$$\begin{aligned}
M_1 &= \mathrm{e}^{2\beta f/\sqrt{\delta}}(f+\alpha)(f\sqrt{\delta} + \hat{d}) + (f\sqrt{\delta} - \hat{d})(f-\alpha),\\
M_2 &= (2\delta - \hat{d}^2)((f+\alpha)\mathrm{e}^{2\beta f/\sqrt{\delta}} - (f-\alpha)),\\
M_3 &= \mathrm{e}^{2\beta f/\sqrt{\delta}}(f+\alpha)(f\hat{d} + 2\sqrt{\delta}) + (f\hat{d} - 2\sqrt{\delta})(f-\alpha).
\end{aligned}$$

Figure 2 shows the basic velocity profiles for $\hat{d} = 0.03$, 0.1, 0.2. The remaining parameters are $\delta = 2.5 \times 10^{-5}$, $\beta = 0.1$ and $\alpha = 0.1$.

Note the significant behaviour of the velocity profiles in figure 2, which is in contrast to the two-layered approach adopted by Chang *et al.* (2006). Because of the nature of the interface conditions between a fluid and a Darcy porous medium, the velocity is always significantly discontinuous there, as is evident in figure 1 of Chang *et al.* (2006). However, our figure 2 shows that this is not the case with our present model. There is still a discontinuity in velocity profile between the Brinkman and Darcy layers, but we can provide an error indicator for this. Let

$$\begin{aligned}
\gamma &= \max\left|\frac{\overline{u}^b - \overline{u}^m}{\overline{u}^m}\right|\\
&= \frac{(\hat{d}^2 - 2\delta)f^2\mathrm{e}^{\beta f/\sqrt{\delta}}}{M_1\sqrt{\delta}} \quad \text{defined at } z = -\beta d_m.
\end{aligned} \tag{2.12}$$

It is easy to show (using the definition of the constant M_1) that β is inversely proportional to the relative error γ. This indicates that the discontinuity of the velocity profile may become numerically significant if the proportion of the porous medium occupied by the transition (β) is too small. We return to analyse (2.12) in § 3.4. All the remaining parameters have negligible impact on γ, within their acceptable ranges.

2.2. *Perturbation equations*

In order to study the instability of the basic solution, we introduce perturbations and non-dimensionalize in an analogous fashion to Chang *et al.* (2006). Although nonlinear disturbances are not addressed in this paper, this would be an interesting subject for future study owing to the potential for subcritical instabilities which are believed to exist in Poiseuille-flow layers (cf. Drazin & Reid 1981).

Squire's theorem is also employed to reduce the three-dimensional problem to an equivalent two-dimensional one, by using a change of variables. Details on this

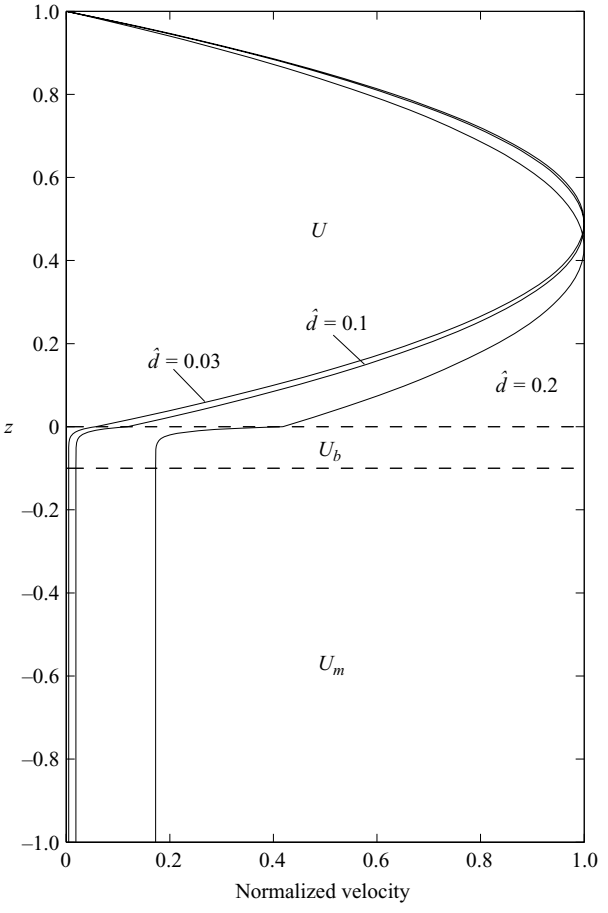

FIGURE 2. Dimensionless basic velocities for the fluid layer (U), the Brinkman layer (U_b) and the Darcy layer (U_m). The dotted lines represent the boundaries between the layers, at $z=0$ and $z=-\beta$.

procedure are similar to those found in Drazin & Reid (1981). During this process we introduce normal modes of the form

$$u_i = u_i(z)\mathrm{e}^{\mathrm{i}(ax+by-act)}, \qquad p = \pi(z)\mathrm{e}^{\mathrm{i}(ax+by-act)},$$

where the streamfunction ψ is defined as $u_1 = \partial\psi/\partial z$, $u_3 = -\partial\psi/\partial x$, with eigenfunction ϕ such that

$$\psi = \phi(z)\mathrm{e}^{\mathrm{i}a(x-ct)}.$$

Similar definitions apply for ψ^b and ψ^m.

In this manner, it can be shown that the tenth-order governing equations have the form

$$(D^2-a^2)^2\phi = Re(U-c)\mathrm{i}a(D^2-a^2)\phi - \mathrm{i}aReU''\phi, \qquad z\in(0,\,1), \quad (2.13a)$$

$$\left(1-\frac{\mathrm{i}a_b c_b Re^b\delta}{\epsilon}-\frac{\delta}{f^2}\left(D_b^2-a_b^2\right)\right)\left(D_b^2-a_b^2\right)\phi^b = 0, \qquad z\in(-\beta,\,0), \quad (2.13b)$$

$$\left(1-\frac{\mathrm{i}a_m c_m Re^m\delta}{\epsilon}\right)\left(D_m^2-a_m^2\right)\phi^m = 0, \qquad z\in(-1,\,-\beta), \quad (2.13c)$$

where the Reynolds numbers Re, Re^b and Re^m correspond to the fluid, Brinkman and Darcy layers, respectively. System (2.13) has been multiplied by δ, which is usually small, to avoid numerical error. In Chang *et al.* (2006) the analogous equation is (2.21). The boundary conditions for the tenth-order system (2.13) at $z=1$ are

$$\phi = D\phi = 0, \tag{2.14}$$

and

$$\phi^m = 0 \tag{2.15}$$

at $z=-1$. On the interface $z=z_b=0$, we have

$$\left.\begin{aligned} Re\phi &= Re^b\phi^b, \\ ReD\phi &= \hat{d}Re^bD_b\phi^b, \\ f^2(D^2+a^2)\phi &= \hat{d}^2\frac{Re^b}{Re}\left(D_b^2+a_b^2\right)\phi^b, \end{aligned}\right\} \tag{2.16}$$

and

$$\begin{aligned} &Re(-\mathrm{i}aRe(U-c)D\phi+(D^2-3a^2)D\phi+U'\mathrm{i}aRe\phi) \\ &\qquad = Re^b\hat{d}^3\left(\frac{1}{f^2}\left(D_b^2-3a_b^2\right)+\frac{\mathrm{i}a_bc_bRe^b}{\epsilon}-\frac{1}{\delta}\right)\phi^b. \end{aligned} \tag{2.17}$$

The final boundary conditions are at the interface $z_m=z_b=-\beta$, where

$$\left.\begin{aligned} Re^b\phi^b &= Re^m\phi^m, \\ D_b^2\phi^b+a_b^2\phi^b &= \frac{\alpha}{\sqrt{\delta}}D_b\phi^b-\frac{\alpha Re^m}{\sqrt{\delta}Re^b}D_m\phi^m, \end{aligned}\right\} \tag{2.18}$$

and

$$Re^b\left(\frac{\mathrm{i}a_bc_bRe^b}{\epsilon}-\frac{1}{\delta}+\frac{1}{f^2}(D_b^2-3a_b^2)\right)D_b\phi^b = Re^m\left(\frac{\mathrm{i}a_mc_mRe^m}{\epsilon}-\frac{1}{\delta}\right)D_m\phi^m \tag{2.19}$$

3. Numerical results

We now solve the eigenvalue problem (2.13)–(2.19) by means of a D^2 Chebyshev tau method. The details are similar to those given by Dongarra, Straughan & Walker (1996). Equations (2.13*a*) and (2.13*b*) are both written as two second-order equations and we solve equations (2.13), not as a tenth-order system, but as five second-order equations. Each of (2.13*a*)–(2.13*c*) is transformed to the Chebyshev domain $(-1, 1)$ and boundary conditions are incorporated (Carr & Straughan 2003). The numerical results have been checked by varying the number of polynomials to verify convergence.

The parameters, unless stated otherwise, are fixed at $\delta=2.5\times10^{-5}$, $\alpha=0.1$, $\beta=0.1$, $\epsilon=0.3$ and $f=\mu/\mu_e=\epsilon$. In § 3.5, f is considered as a free parameter. These values have been chosen to be consistent with a porous-layer depth of 3 cm so that a direct comparison can be made with Chang *et al.* (2006), and the experiments of Goharzadeh *et al.* (2005). Although most of the results are derived for a small-scale porous medium, which is highly relevant to practical experimentation, § 3.3 studies length scales of up to 1 m in the context of geological and industrial applications (Straughan 2002; Nield & Bejan 2006). This is achieved by adopting realistic values for the permeabilities of soil and Foametal (which is used extensively in industrial applications such as heat exchangers, chemical reactors and fluid filters).

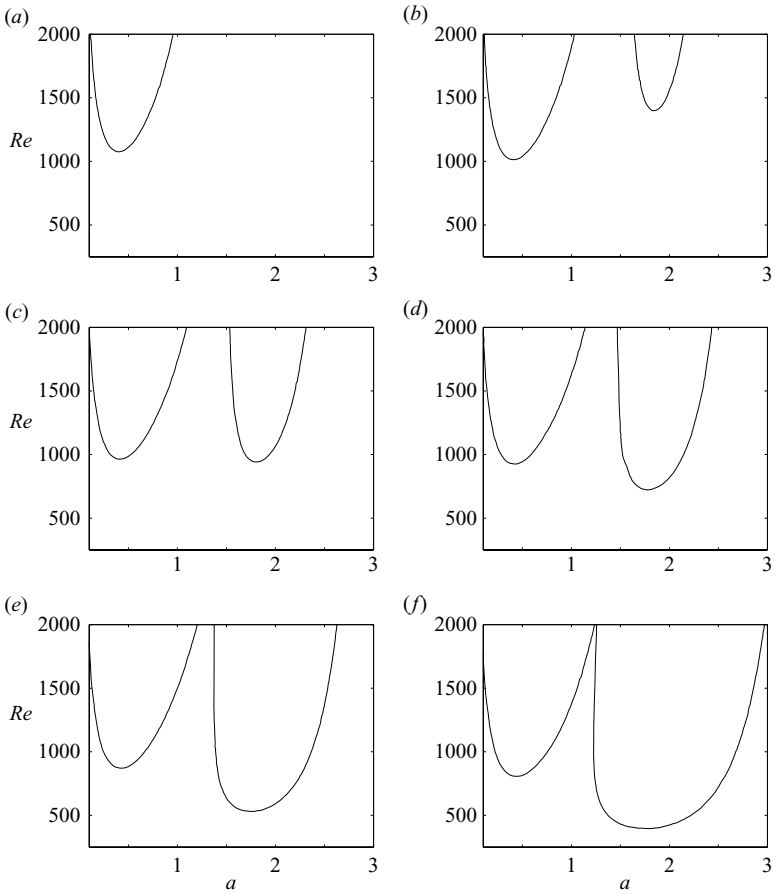

FIGURE 3. Critical Reynolds number against wavenumber with several assigned values of depth ratio; (*a*) $\hat{d} = 0.03$, (*b*) $\hat{d} = 0.032$, (*c*) $\hat{d} = 0.034$, (*d*) $\hat{d} = 0.038$, (*e*) $\hat{d} = 0.04$, (*f*) $\hat{d} = 0.05$. The remaining parameters are $\delta = 2.5 \times 10^{-5}$, $\alpha = 0.1$, $\beta = 0.1$ and $\epsilon = 0.3$.

3.1. *Depth ratio $\hat{d}$ effects*

The change from dominance by the porous layer to dominance by the fluid layer is found in the range $\hat{d} \in (0.032, 0.036)$. This is very different from that of Chen & Chen (1988) who found the changeover was for $\hat{d} = O(0.13)$. In fact, Chang *et al.* (2006) also found critical $\hat{d}$ values in the same range. This suggests that Poiseuille-flow problems may behave very differently from those of thermal convection, i.e. the transition layer for Poiseuille flow may well be larger.

In figure 3(*a*), $\hat{d} = 0.03$ and we see the instability dominated by one mode, the porous mode. As we increase $\hat{d}$ to $\hat{d} = 0.032$ (see figure 3*b*), the fluid mode appears. As $\hat{d}$ is increased (figure 3*c*, *d*), the fluid mode moves down and eventually dominates the instability. In figure 3(*e*, *f*), this behaviour continues as $\hat{d}$ is increased. Figure 4 shows the eigenfunctions (streamfunctions) as $\hat{d}$ crosses through the changeover point. When $\hat{d} = 0.03$, the porous mode dominates. We see a flow reversal at the interface which is consistent with what is found by Chang *et al.* (2006). In figure 4(*b*), the fluid mode is totally dominant and flow reversal (for the real part of the eigenfunction) is not present.

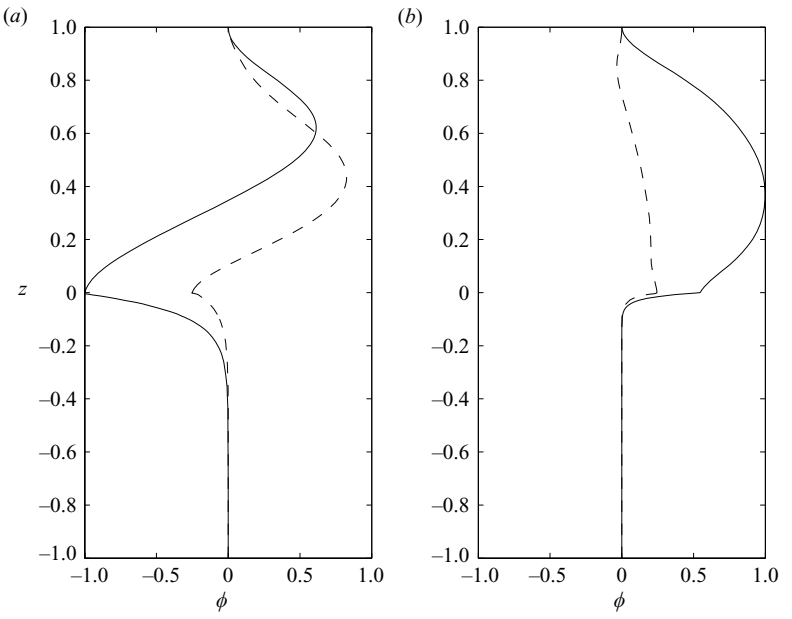

FIGURE 4. Normalized streamfunction with respect to two depth ratios at a critical state, where (*a*) $\hat{d} = 0.03$, $a_c = 0.4$, $Re_c = 1075$, and (*b*) $\hat{d} = 0.034$, $a_c = 1.8$, $Re_c = 942$. The solid and dashed lines represent the real and imaginary parts, respectively. The remaining parameters are $\delta = 2.5 \times 10^{-5}$, $\alpha = 0.1$, $\beta = 0.1$ and $\epsilon = 0.3$.

Before moving on to variation in porosity, note that varying the coefficient α had a negligible effect.

3.2. *Porosity ϵ effects*

The neutral curves for varying the porosity are shown in figure 5. In figure 5(*a*), the porous mode dominates although the fluid mode is present. In figures 5(*b*) to 5(*d*), where the porosity increases, the fluid mode moves down and eventually dominates the instability.

3.3. *Porous-layer depth d_m effects*

In figure 6, we show the effects of the porous-layer depth on the critical $\hat{d} = d/d_m$ value (i.e. where the instability switches between the porous and fluid layers). This is achieved by defining the permeability κ of the porous medium to represent soil ($\kappa = 1.8 \times 10^{-10}\,\mathrm{m}^2$) and Foametal ($\kappa = 8.19 \times 10^{-8}\,\mathrm{m}^2$), respectively (cf. Straughan 2002; Nield & Bejan 2006), and varying $\delta = \kappa^2/d_m$. Since δ is a dimensionless quantity, the graphs for soil and Foametal are derived from a single set of results, where d_m simply needs to be rescaled in accordance with the relevant permeability.

It is clear from figure 6 that as the porous-layer depth d_m is increased, the critical $\hat{d}$ value decreases. As we would expect, the results show that a higher permeability corresponds to a higher critical $\hat{d}$ value.

Note that the neutral curves are identical for all the porous-layer depths at their corresponding critical $\hat{d}$. This indicates that the results for the 3 cm layer are applicable to other depths and permeabilities.

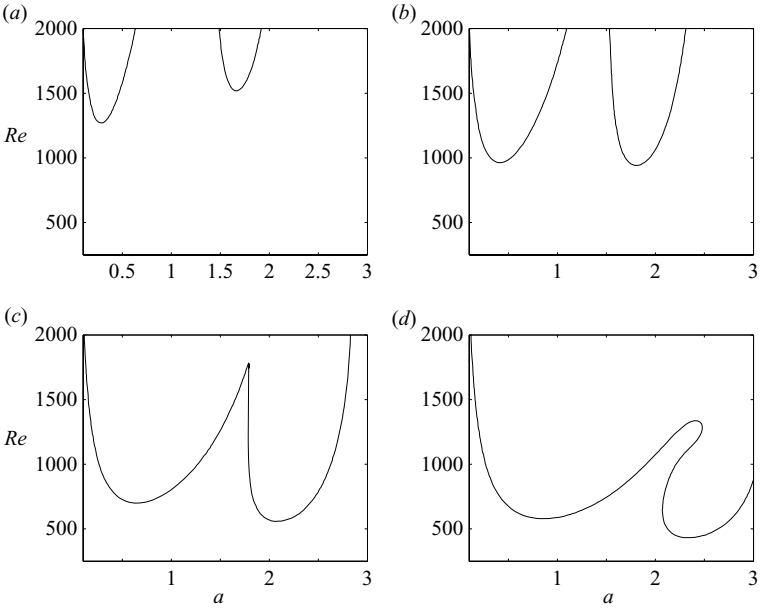

FIGURE 5. Critical Reynolds number against wavenumber with several assigned values of porosity; (*a*) $\epsilon = 0.2$, (*b*) $\epsilon = 0.3$, (*c*) $\epsilon = 0.5$, (*d*) $\epsilon = 0.7$. The remaining parameters are $\hat{d} = 0.034$, $\delta = 2.5 \times 10^{-5}$, $\alpha = 0.1$ and $\beta = 0.1$.

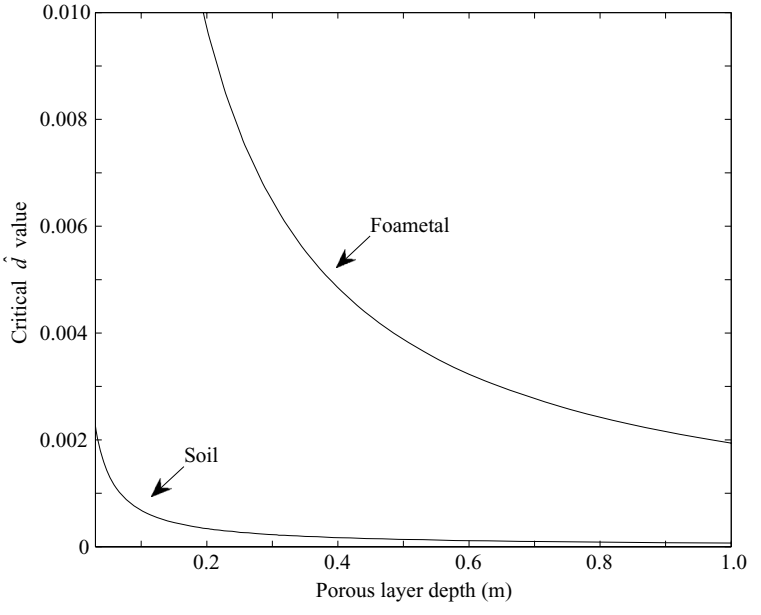

FIGURE 6. Critical $\hat{d}$ against porous layer depth d_m. The Foametal and soil graphs refer to fixed permeabilities κ of 8.19×10^{-8} m^2 and 1.8×10^{-10} m^2, respectively.

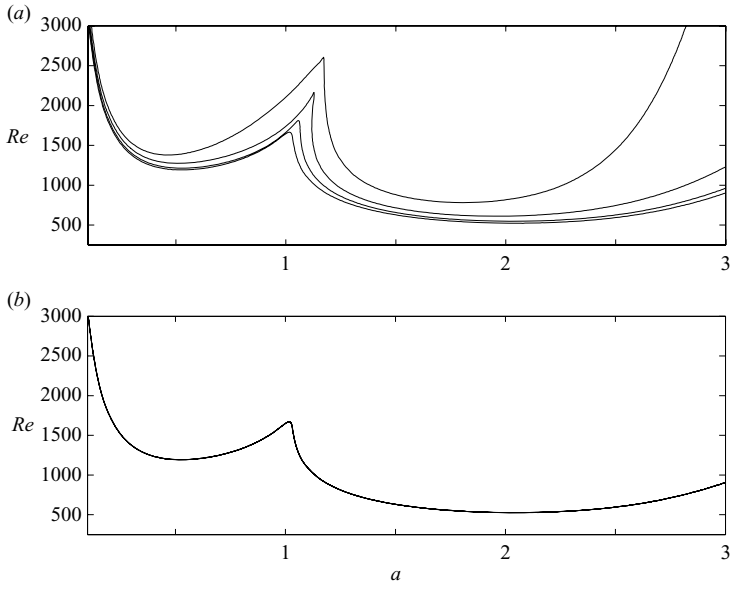

FIGURE 7. Critical Reynolds number against wavenumber with several assigned values of β; in descending order the neutral curves are (*a*) $\beta = 0.001,\ 0.005,\ 0.01,\ 0.05$, (*b*) $\beta = 0.1,\ 0.15,\ 0.2,\ 0.3$. The remaining parameters are $\hat{d} = 0.13$, $\epsilon = 0.3$, $\delta = 2.5 \times 10^{-5}$ and $\alpha = 0.1$.

3.4. *Transition-layer effects*

In figure 7, we show the effects of varying the Brinkman-layer depth parameter, β. This parameter has a major effect on instability.

If we consider a Poiseuille flow in the experimental situation of Chen & Chen (1988) where the total depth was 3 cm and the porous medium was composed of 3 mm glass beads, then, using the results of Goharzadeh *et al.* (2005) which predicts $\beta d_m/D = \delta_1/D = O(1)$, we expect a value of β in the region of 0.1. In figure 7, we present the neutral curves for β varying from 1×10^{-3} to 0.3. (The computations are difficult for β very small and we were unable to compute $\beta \to 0$ to see whether we recover the results of Chang *et al.* (2006), although our computations do reproduce the numerical results of Chang *et al.* (2006) when we take $\beta = 0$ and study the fluid-/Darcy-layer problem.)

In figure 7(*a*), we see that for β increasing between 1×10^{-3} and 0.05, the fluid dominance effect is amplified, such that the porous mode is effectively removed by increasing the depth of the Brinkman layer.

Recalling that the relative error of the velocity profile at the Brinkman/Darcy interface γ is defined in (2.12), we find that $\gamma \in (4.25,\ 22.53)$ for $\beta \in (0.001,\ 0.01)$, but $\gamma \in (6\ \times 10^{-14},\ 0.05)$ for $\beta \in (0.05,\ 0.3)$. Therefore, we see that if β is taken large enough to make the discontinuity of the velocity profile numerically insignificant, increasing β beyond this point makes negligible change to the neutral curve, which is reflected in figure 7(*b*). The value of β was taken to be 0.1 throughout the paper as this forced the discontinuity of the velocity profile to be numerically insignificant, which was one of the main aims of this paper.

3.5. *Viscosity ratio μ/μ_e effects*

The neutral curves for a wide range of the viscosity ratio $f = \sqrt{\mu/\mu_e}$ are shown in figure 8. In figure 8(*a*), the fluid mode dominates although the porous mode is

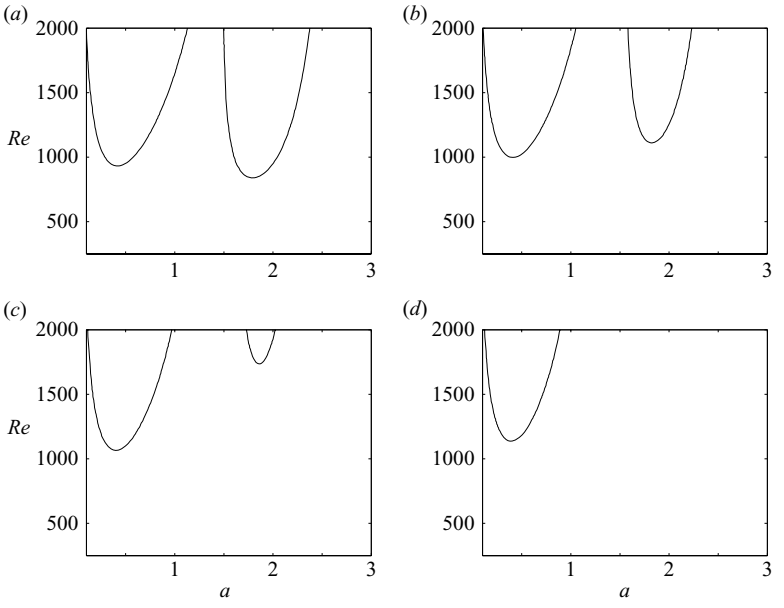

FIGURE 8. Critical Reynolds number against wavenumber with several assigned values of $f = \sqrt{\mu/\mu_e}$; (*a*) $f = 0.5$, (*b*) $f = 0.6$, (*c*) $f = 0.7$, (*d*) $f = 0.8$. The remaining parameters are $\hat{d} = 0.034$, $\epsilon = 0.3$, $\beta = 0.1$ and $\alpha = 0.1$.

present. The porous mode completely dominates as f is increased. In the context of the relatively large range of f studied, these results indicate that if the predictions of ratio f are close in value, it may be taken as constant, but if there is substantial variation this clearly may affect the neutral curve. For example, it was found for the results shown in this paper that the Whitaker formula ($\mu/\mu_e = \epsilon$) and the Einstein formula ($\mu_e/\mu = 1 + 5/2(1-\epsilon)$), generate values of f which are close enough in value to cause an insignificant impact on the neutral curve.

This work was supported by a Research Project Grant of the Leverhulme Trust - grant F/00128/AK.

REFERENCES

BEAVERS, G. S. & JOSEPH, D. D. 1967 Boundary conditions at a naturally permeable wall. *J. Fluid Mech.* **30**, 197–207.

BUTLER, K. M. & FARRELL, B. F. 1992 Three-dimensional optimal perturbations in viscous shear flow. *Phys. Fluids* A **4**, 1637–1650.

CARR, M. 2004 Penetrative convection in a superposed porous-medium-fluid layer via internal heating. *J. Fluid Mech.* **509**, 305–329.

CARR, M. & STRAUGHAN, B. 2003 Penetrative convection in a fluid overlying a porous layer. *Adv. Water Resources* **26**, 263–276.

CHANG, M. 2005 Thermal convection in superposed fluid and porous layers subjected to a horizontal plane Couette flow. *Phys. Fluids* **17**, 064106-1–064106-7.

CHANG, M. 2006 Thermal convection in superposed fluid and porous layers subjected to a plane Poiseuille flow. *Phys. Fluids* **18**, 035104-1–035104-10.

CHANG, M., CHEN, F. & STRAUGHAN, B. 2006 Instability of Poiseuille flow in a fluid overlying a porous layer. *J. Fluid Mech.* **564**, 287–303.

Chen, F. & Chen, C. F. 1988 Onset of finger convection in a horizontal porous layer underlying a fluid layer. *Trans. ASME* C: *J. Heat Transfer* **110**, 403–409.

Choi, C. Y. & Waller, P. M. 1997 Momentum transport mechanism for water flow over porous media. *J. Environ. Engng* **123**, 792–799.

Das, D. B., Nassehi, V. & Wakeman, R. J. 2002 A finite volume model for the hydrodynamics of combined free and porous flow in sub-surface regions. *Adv. Environ. Res.* **7**, 35–58.

Discacciati, M., Miglio, E. & Quarteroni, A. 2002 Mathematical and numerical models for coupling surface and groundwater flows. *Appl. Numer. Maths* **43**, 57–74.

Dongarra, J. J., Straughan, B. & Walker, D. W. 1996 Chebyshev tau-QZ algorithm methods for calculating spectra of hydrodynamic stability problems. *Appl. Numer. Maths* **22**, 399–435.

Drazin, P. G. & Reid, W. H. 1981 *Hydrodynamic Stability*. Cambridge University Press.

Friedlander, S. & Howard, L. 1998 Instability in parallel flows revisited. *Stud. Appl. Maths* **101**, 1–21.

Goharzadeh, A., Khalili, A. & Jorgensen, B. B. 2005 Transition layer at a fluid–porous interface. *Phys. Fluids* **17**, 057102-1–057102-10.

Goyeau, B., Lhuillier, D., Gobin, D. & Velarde M. G. 2003 Momentum transport at a fluid–porous interface. *Intl J. Heat Mass Trans.* **46**, 4071–4081.

Gustavsson, L. 1986 Excitation of direct resonances in plane Poiseuille flow. *Stud. Appl. Maths* **75**, 227–248.

Hirata, S. C., Goyeau, B., Gobin, D., Carr, M. & Cotta, R. M. 2007 Linear stability of natural convection in superposed fluid and porous layers: influence of the interfacial modelling. *Intl J. Heat Mass Transfer* **50**, 1356–1367.

Jones, I. P. 1973 Low Reynolds number flow past a porous spherical shell. *Proc. Camb. Phil. Soc.* **73**, 231–238.

Lu, J. & Chen, F. 1997 Assessment of mathematical models for the flow in directional solidification. *J. Crystal Growth* **171**, 601–613.

Miglio, E., Quarteroni, A. & Saleri, F. 2003 Coupling of free surface and groundwater flows. *Computers Fluids* **32**, 73–83.

Nield, D. A. 1977 Onset of convection in a fluid layer overlying a layer of porous medium. *J. Fluid Mech.* **81**, 513–522.

Nield, D. A. 1983 The boundary correction for the Rayleigh–Darcy problem: limitations of the Brinkman equation. *J. Fluid Mech.* **128**, 37–46.

Nield, D. A. 1991 The limitations of the Brinkman–Forchheimer equation in modeling flow in a saturated porous medium and at an interface. *Intl J. Heat Fluid Flow* **12**, 269–272.

Nield, D. A. 1998 Modelling the effect of surface tension on the onset of natural convection in a saturated porous medium. *Transport Porous Media* **31**, 365–368.

Nield, D. A. & Bejan, A. 2006 *Convection in Porous Media*, 3rd edn. Springer.

Ochoa-Tapia, J. A. & Whitaker, S. 1995 Momentum transfer at the boundary between a porous medium and a homogeneous fluid I. Theoretical development. *Intl J. Heat Mass Transfer* **38**, 2635–2646.

Straughan, B. 1998 *Explosive Instabilities in Mechanics*. Springer.

Straughan, B. 2002 Effect of property variation and modelling on convection in a fluid overlying a porous layer. *Intl J. Numer. Anal. Meth. Geomech.* **26**, 75–97.

Whitaker, S. 1986 Flow in porous media I: a theoretical derivation of Darcy's law. *Transport Porous Media* **1**, 3–25.